Heliyon 10 (2024) e26621

Contents lists available at ScienceDirect

Heliyon

journal homepage: www.cell.com/heliyon

Research article

Surface micropatterning of 3D printed PCL scaffolds promotes osteogenic differentiation of BMSCs and regulates macrophage M2 polarization

Weihua Huang [a,b,c,d,†], Xiayu Cai [a,c,†], Chujie Xiao [a,c,e], Wenlu Song [a,c,f], Huinan Yin [d], Weikang Xu [a,c,g,1,*]

[a] *Institute of Biological and Medical Engineering, Guangdong Academy of Sciences, Jianghai Avenue Central, Haizhu District, Guangzhou, Guangdong, 510316, China*

[b] *Department of Orthopaedic Surgery, Affiliated Qingyuan Hospital, Guangzhou Medical University, Qingyuan People's Hospital, No.35, Yinquan North Road, Qingcheng District, Qingyuan, Guangdong, 511518, China*

[c] *National Engineering Research Center for Healthcare Devices, Guangdong Key Lab of Medical Electronic Instruments and Polymer Material Products, Guangdong Institute of Medical Instruments, No. 1307 Guangzhou Avenue Central, Tianhe District, Guangzhou, Guangdong, 510500, China*

[d] *Department of Orthopaedic Surgery, The Second Affiliated Hospital of Guangzhou Medical University, The Second Clinical Medicine School of Guangzhou Medical University, No. 250, Changgang East Road, Haizhu District, Guangzhou, Guangdong, 510260, China*

[e] *National Engineering Research Center for Human Tissue Restoration and Function Reconstruction, South China University of Technology, Wushan Road 381, Guangzhou, Guangdong, 510275, China*

[f] *Sun Yat-Sen University, Xingang West Road 135, Guangzhou, Guangdong, 510006, China*

[g] *Guangdong Chinese Medicine Intelligent Diagnosis and Treatment Engineering Technology Research center, Jianghai Avenue Central, Haizhu District, Guangzhou, Guangdong 510316, China*

ARTICLE INFO

Keywords:
Grating micropatterning
PCL
BMSCs
Osteogenic differentiation
Immunoregulation

ABSTRACT

Micropatterned structures on the surface of materials possessing biomimetic properties to mimic the extracellular matrix and induce cellular behaviors have been widely studied. However, it is still a major challenge to obtain internally stable and controllable micropatterned 3D scaffolds for bone repair and regeneration. In this study, 3D scaffolds with regular grating arrays using polycaprolactone (PCL) as a matrix material were prepared by combining 3D printing and soft lithography, and the effects of grating micropatterning on osteogenic differentiation of BMSCs and M1/M2 polarization of macrophages were investigated. The results showed that compared with the planar group and the 30um grating spacing group, PCL with a grating spacing of 20um significantly promoted the osteogenic differentiation of BMSCs, induced the polarization of RAW264.7 cells toward M2 type, and suppressed the expression of M1-type pro-inflammatory genes and markers. In conclusion, we successfully constructed PCL-based three-dimensional scaffolds with stable and controllable micrographs (grating arrays) inside, which possess excellent osteogenic properties and promote the formation of an immune microenvironment conducive to osteogenesis. This study is a step forward to the exploration of bone-filling materials affecting cell behavior, and makes a new contribution to the provision of high-quality materials.

* Corresponding author. Institute of biological and Medical Engineering, Guangdong Academy of Sciences, Jianghai Avenue Central, Haizhu District, Guangzhou, Guangdong 510316, China.

E-mail addresses: xuweikang8700@aliyun.com, 759200816@qq.com (W. Xu).

[1] Present address: Jianghai Avenue Central, Haizhu District, Guangzhou, Guangdong 510316, China.

[†] These authors contributed equally to this work.

https://doi.org/10.1016/j.heliyon.2024.e26621

Received 4 February 2024; Received in revised form 14 February 2024; Accepted 16 February 2024

Available online 22 February 2024

1. Introduction

Bone marrow mesenchymal stem cells (BMSCs) can further differentiate into osteoblasts and osteocytes, which have great osteogenic potential and play an important role in the deposition of calcium nodules in the regeneration of bone defects and the promotion of bone matrix formation [1,2]. In addition, the bone regeneration process cannot be separated from a suitable immune microenvironment [3]. In a recent study, Minhao Wu et al. showed that it is particularly important for biomedical materials to have the ability to immunomodulate macrophage M1 to M2 polarization [4]. It was mentioned in the study that the formation of an immune microenvironment enriched with M2-type macrophages plays a positive role in clearing the non-specific inflammation mediated by M1-type macrophages at the early stage of bone repair, which is conducive to stimulating the angiogenesis of the grafts and inducing osseointegration. Therefore, most of the bone tissue engineering materials will undergo surface modification of the material, such as physical modification or grafting of certain chemical groups, and the purpose of the modification is to enable the implant and the host to produce a positive biological response, guiding the cell proliferation, adhesion, migration, and differentiation, to obtain a better osseointegration and osteoinduction properties [5,6].

The adhesion behavior of cells is influenced by many factors, such as the surface properties of the material, compared to smooth surfaces, the micropatterned structure of the material surface can mimic the extracellular matrix and provide better cell adhesion sites, therefore, the role of surface patterning of materials on cell adhesion has received great attention [7–9]. The most obvious effect of surface micropatterning on cell adhesion function is reflected in the effect on cell geometry, where many cell types (e.g., BMSCs, macrophages, etc.) are usually adjusted their migration directions at different surface microscopes, such as gratings, columns, or lines [10]. For example, Wang J et al. found that BCP ceramics possessing surface micropatterns could promote osteogenic differentiation of pre-matrix cells as well as induce macrophage polarization towards M2 type [11]. The topology of the material surface influences the fate of cell proliferation and differentiation [12]. However, most of the current studies on surface micropatterning to regulate cell behavior are at the two-dimensional level, ignoring the fact that the natural extracellular matrix is a carrier with a three-dimensional topology [13]. Although there are individual studies conducted to try the corresponding surface-morphing scaffolds for tissue regeneration, such as 3D printed porous tantalum with surface microporous nanostructures and polymer scaffolds with ECM-like nanofibrous morphology structures [14,15]. These scaffolds soak in liquid in the form of solute exchange, which increases the specific surface area of scaffolds, and provides some reference for scaffolds using related techniques to coordinate multiple cells for bone regeneration. However, due to technological limitations, it is still challenging to realize controllable surface micropatterns inside the scaffolds. Various techniques, including photolithography, machining, 3D printing, and melt electrospinning printing, have been used in combination with conventional preparation methods to obtain tissue scaffolds with controllable microstructure and surface morphology [16–21]. For example, Jonelle Z. Yu et al. investigated the correspondence of human neonatal fibroblasts (NHFs) on different sizes of wavy gelatin-chondroitin-6-sulfate-hyaluronic acid hydrogel scaffolds and found that the cells preferentially aligned themselves to curvilinear positions of the fluctuating microtopography [18].

Polycaprolactone (PCL) is approved for clinical use by the U.S. Food and Drug Administration (FDA) and is widely used in bone tissue engineering research. Compared with other materials, PCL possesses slow degradation properties, which provide sufficient time for bone defect repair [22]. Meanwhile, it has been shown that the regular grating microstructure on the surface of the material is more capable of guiding the migratory adhesion behavior of the cells than the planar or micropillar structure [23]. Unfortunately, there are few reports of PCL-based grating microstructures on the surface of 3D-printed scaffolds regulating the osteogenic differentiation of BMSCs and M1/M2 polarization of macrophages.

The effects of micropatterns with 20–50 μm size intervals on bone marrow MSCs have been studied in the literature [24–26], as well as the effects of micropatterns with 40–100 μm size intervals on human macrophages [27]. However, few literature reports have reported the modulatory effects on both rat bone marrow MSCs and mouse macrophages. In particular, the size of mouse macrophages is about 20 μm. Therefore, two sizes, 20 μm and 30 μm, were further selected in this work to investigate the regulatory effects of micropatterns on cells, especially mouse macrophages. Here, we prepared PCL lamellar scaffolds with regular grating arrays using 3D printing combined with soft lithography and obtained three-dimensional scaffolds with controlled grating structures inside by layer-by-layer stacking and localized high-temperature spot welding. The effects of grating array micropatterning on the proliferation and differentiation of BMSCs and the ability to regulate the polarization of macrophages toward M1 or M2 were investigated. The results showed that PCL scaffolds with internal adjustable micropatterns could effectively promote osteogenic differentiation, inhibit the expression of macrophage M1-type pro-inflammatory genes, and up-regulate macrophage M2-type related anti-inflammatory repair genes, with good induction of pro-osteoporotic repair and regeneration and immunomodulatory functions. Our study achieves a shift from 2D micropatterned studies to 3D studies, contributing to the modulation of cellular behavior by bone-filling materials.

2. Materials and methods

2.1. Materials

PCL (Molecular weight: 54,000 Da), cetylpyridinium chloride (CPC) was obtained from Sigma-Aldrich. A negative photoresist (SU-8) was purchased from MICROCHEM. ITO glass was obtained from (Chunghwa Picture Tubes Co., Ltd.). Polydimethylsiloxane (PDMS) was from Dow Corning. Fetal bovine serum, RPMI1640, double antibody, DMEM (4.5 high-glucose), 10× trypsin-EDTA was purchased from Gibco. IFN-γ, IL-4, IL-13 (Peprotech), Calcein-AM/PI Double Staining kit, and Cell Counting Kit-8 (CCK-8) were from Tongren

Chemical. Vitamin C and sodium β-glycerophosphate were purchased from Maclean's, and dexamethasone was from J&amp K Scientific. BMSCs and RAW264.7 cells were supplied by ATCC (U.S.A.). Ultrapure RNA Kit, Hi-Fi Script cDNA Synthesis Kit, and Ultra SYBR Mixture (Low ROX) were supplied by CWBIO. LPS, Osteoblast Mineralized Nodule Staining Kit (Alizarin Red S Method) ALP Kit, BCA Protein Assay Kit, and RIPA Lysate were obtained from Biyun Tian Biotechnology Co., Ltd.

2.2. Preparation of PCL surface microforms

2.2.1. Preparation of PCL die sheet

To the dry ITO glass, 1 ml of negative photoresist SU-8 was added dropwise and coated uniformly, and a highly flat surface coating was obtained on the glass surface by centrifugal glue dumping method. The finished samples were dried on a glue dispenser (BP–2B, Beijing Heshixingye Technology Co., Ltd.) and fixed on a photolithography machine (Institute of Photovoltaic Technology, Chinese Academy of Sciences) to be exposed (using CorelDraw software to design grating arrays of 20 μm and 30 μm in size, with a graphic area of 25.6 mm × 20.8 mm). After exposure, the glass samples were dried again, and the desired micropatterns were obtained by developing with NaOH, fixing with isopropyl alcohol, and drying. The prepared sample was placed in a Petri dish, and the PDMS host agent and curing agent were poured in, vacuumed, and placed in an oven at 70 °C to cure the PDMS to obtain a PDMS template with grating micropatterns on the surface (10:1 wt ratio of PDMS to curing agent). The PDMS micropatterned template was placed on a thermostatic heating stage (MS7-H550-S, DWB) and heated to 95 °C. A smooth PCL film was lightly placed on the surface of the PDMS micropatterned template and another piece of the same micropatterned template was wrapped around the PCL film, and after cooling and peeling off the film, PCL films with grating arrays of different sizes (G20, G30) were obtained. PCL planar group films (Flat) were obtained in the same way using a smooth PDMS template.

2.2.2. Preparation of 3D PCL scaffolds

A 2D square slice unit of size 10 × 10 mm was designed as the 3D printing path map using the 3D drawing software Solid Works. The path map in stl format was imported into a 3D printer (EFL-BP-6603, Suzhou Institute of Intelligent Manufacturing). The PCL raw material was put into the cylinder, heated, and melted to print the 2D scaffold slice layer with a filament diameter of 400um and a fiber pitch of 600um. The grating micro-patterned and smooth-surface PDMS template was placed on a heating plate at 75 °C. The printed 2D scaffold layer was lightly placed on the PDMS surface, and the corresponding PDMS template was pressed to obtain the planar PCL scaffold layer (Flat) and PCL scaffold layers with micro-patterned structures on both sides (G20, G30). The obtained scaffold layers were stacked layer by layer, and then the layers were connected by high-temperature spot hot-melting to finally obtain the scaffolds with controllable micro-patterned structures on the internal surfaces.

2.3. Material characterization

The surface topographic structure of the material was characterized by high-resolution field emission scanning electron microscopy (SEM, Merrill Carl Zeiss, Germany). The size of the micro-patterns on the PCL surface as well as the size of the boundaries between the micro-patterns were statistically analyzed using Image J software. The microscopic nano-surface morphology and roughness of the PCL film samples were characterized by atomic force microscopy (AFM, Asylum Research, American) for characterization. During the testing, the surface morphology and roughness of the sample surface of 10 μm × 10 μm size area were tested by choosing the tapping mode.

2.4. Porosity testing of materials

The mass of the dried sample was measured and recorded as M0. The total mass of the specific gravity bottle filled with anhydrous ethanol at room temperature was recorded as M1. The total mass of the sample placed in the specific gravity bottle and measured after ultrasonication to exhaust the air bubbles was recorded as M2. The sample was taken out and weighed to obtain the residual mass which was recorded as M3.The formula for calculating the porosity of the material was given as:

$$P = (M2 - M3 - M0)/(M1 - M3)$$

2.5. Shear strength test of materials

Epoxy resin adhesive was used to fix both ends of the stent on the polystyrene sheet, and the tensile shear test was carried out through the universal testing machine, the tensile speed was 10 mm/min. Each set of samples was repeated 3 times to obtain the shear strength as mean ± standard deviation.

2.6. Cellular experiments

2.6.1. Cell culture

In this study, RAW264.7 cells and BMSCs from the mouse monocyte-macrophage cell line were mainly used for experiments. RPMI 1640, DMEM with 10% FBS, 100 μg/mL penicillin, and 100 μg/mL streptomycin were used to form a complete medium, respectively. The cells were cultured in a humidified thermostatic cell culture incubator at 37 °C with a CO_2 concentration of 5%. The medium was

changed daily or bi-daily during the incubation process depending on the cell condition. Cells were passaged at 70–80% fusion of cell growth. All cell generations used in this experiment were 3–5 generations.

Materials were sterilized by irradiation before cell inoculation and subsequently fixed in well plates and immersed overnight in a complete medium at 37 °C, 5% CO_2 incubator.

2.6.2. Cell proliferation and activity

Briefly, sterilized Falt, G20, and G30 sets of samples were placed in 48-well plates, in which samples were seeded with 1×10^4 BMSCs or 2×10^4 RAW264.7 cells. After 1, 3, 5, and 7 d of incubation the medium was removed and the OD values of cells on on the different samples were determined by a microplate reader (Tecan Spark, Austria).

Cell growth viability assay of BMSCs and RAW264.7 cells was detected by live/dead staining method. The material was removed from the well plate and the cells were washed well with PBS for 2–3 times to fully remove the residual esterase activity. Take 150 μL of staining working solution and add it into the inner to the material, incubate at 37 °C for 15 min. The morphological state and distribution of cells on the sample surface were observed and photographed using an inverted fluorescence microscope. The test time was chosen to be carried out after the cells had adhered and proliferated on the sample surface for 72h.

2.6.3. Osteogenic differentiation of BMSCs

2×10^4 BMSCs were added to 48-well plates containing the samples, and after 24 h of incubation, the supernatant was aspirated and discarded, and the osteogenic induction culture (100 ml of finished cultivation, 0.39 mg of dexamethasone, 1.76 mg of vitamin C, 306.11 mg of sodium β-glycerophosphate) was added and changed periodically. After 7 and 14 days of osteogenic induction culture, the induction was terminated, and real-time fluorescence quantitative PCR was used to detect the osteogenic marker genes Collagen type I (COLI), Runt-related Transcription Factor 2 (RUNX2), alkaline phosphatase (RUNX1), and alkaline phosphatase (RUNX2). Collagen type I (COLI), Runt-related Transcription Factor 2 (RUNX2), alkaline phosphatase (ALP), in the cells, and glyceraldehyde phosphate dehydrogenase (GAPDH) were used as the internal reference gene. Table 1 shows the sequences of the genes detected in the cells. Table 1 shows the sequences of the genes detected.

2.6.4. Macrophage polarization gene expression level detection

RAW264.7 cells were inoculated onto 48-well plate samples at a density of 5×10^4 cells per well. After 12 h of cell adhesion, the complete culture medium in the well plates was replaced with a complete medium containing M2 stimulating factors (10 ng/ml IL-4 and 4 ng/ml IL-13) or M1 stimulating factors (200 ng/ml LPS and 5 ng/ml IFN-γ) for 12 h. After the stimulation was completed, the stimulating solution was aspirated, washed with PBS and then added to the complete medium, and incubated for 3 and 5 days. Real-time fluorescence quantitative PCR was used to detect the M2 immunomarker genes interleukin 10 (IL-10), Arginase (Arg), transforming growth factor-β_1 (TGF-β1), and the M1 immunomarker genes Tumor necrosis factor-α (TNF-α), Inducible Nitric Oxide Synthase (iNOS), with GAPDH as an internal reference gene. Table 2 shows the sequences of the genes detected.

2.6.5. Macrophage flow cytometry experiments

RAW264.7 cells were inoculated onto 48-well plate samples at a density of 5×10^4 cells per well. After 12 h of cell adhesion, the complete culture medium in the well plate was replaced with a complete medium containing M2 stimulating factor or a complete medium containing M1 stimulating factor for 12 h. After the stimulation was completed, the stimulating solution was aspirated, and the complete medium was washed with PBS and added again for a total of 1 day. Macrophage surface marker proteins were labeled with CD206 or CD11c and detected using flow cytometry.

2.6.6. Statistical analysis

All statistical analyses were processed using GraphPad Prism software. One-way analysis of variance (ANOVA) followed by Dunnett's multiple comparison test was used to determine significant differences between the experimental groups. $p < 0.05$ was considered statistically significant.

Table 1
Primers used in real-time quantification of selected osteogenic marker gene transcripts.

Gene transcript	Forward primer sequence	Reverse primer sequence
GAPDH	GCCATGAGGTCCACCACCCT	AAGGTCATCCCAGAGCTG
COLI	TTCTCCTGGCAAAGACGGAC	CTCAAGGTCACGGTCACGAA
RUNX2	TCGGAGAGGTACCAGATGGG	AGGTGAAACTCTTGCCTCGT
ALP	GGAGATGGTATGGGCGTCTC	GGACCTGAGCGTTGGTGTTA

ALP enzyme activity was assayed on days 7 and 14 using the BCA method, and calcium nodule staining using alizarin red S and quantification of calcium nodules by 10% CPC were performed on day 14.

Table 2
Primers used in real-time quantification of selected Immunomarker gene transcripts.

Gene transcript	Forward primer sequence	Reverse primer sequence
GAPDH	GCCATGAGGTCCACCACCCT	AAGGTCATCCCAGAGCTG
IL-10	GGTGAGAAGCTGAAGACCCT	CACTCTTCACCTGCTCCACTG
Arg	CATATCTGCCAAAGACATCG	CATATCTGCCAAAGACATCG
TGF-β1	TGGAGCAACATGTGGAACTC	TGCCGTACAACTCCAGTGAC
TNF-α	CAACGGCATGGATCTCAAAG	CAGCCTTGTCCCTTGAAGA
iNOS	ATGCTACTGGAGGTGGGTG	GATGTTGTAGCGCTGTGTGT

3. Results

3.1. Characterization of materials

SEM was used to characterize the micropatterns on the PCL surface, and the surface morphology of the samples is shown in Fig. 1. A. Compared with the Flat group, the G20 and G30 groups have a regular grating array structure, and there are no obvious defects as well as impurities on the grating surface. Image J software was used to statistically analyze the different micropatterns and the results are shown in Fig. 1. B. The grating spacing sizes of the G20 and G30 groups are 21.60 ± 0.56μm and 30.76 ± 0.72μm, respectively, and

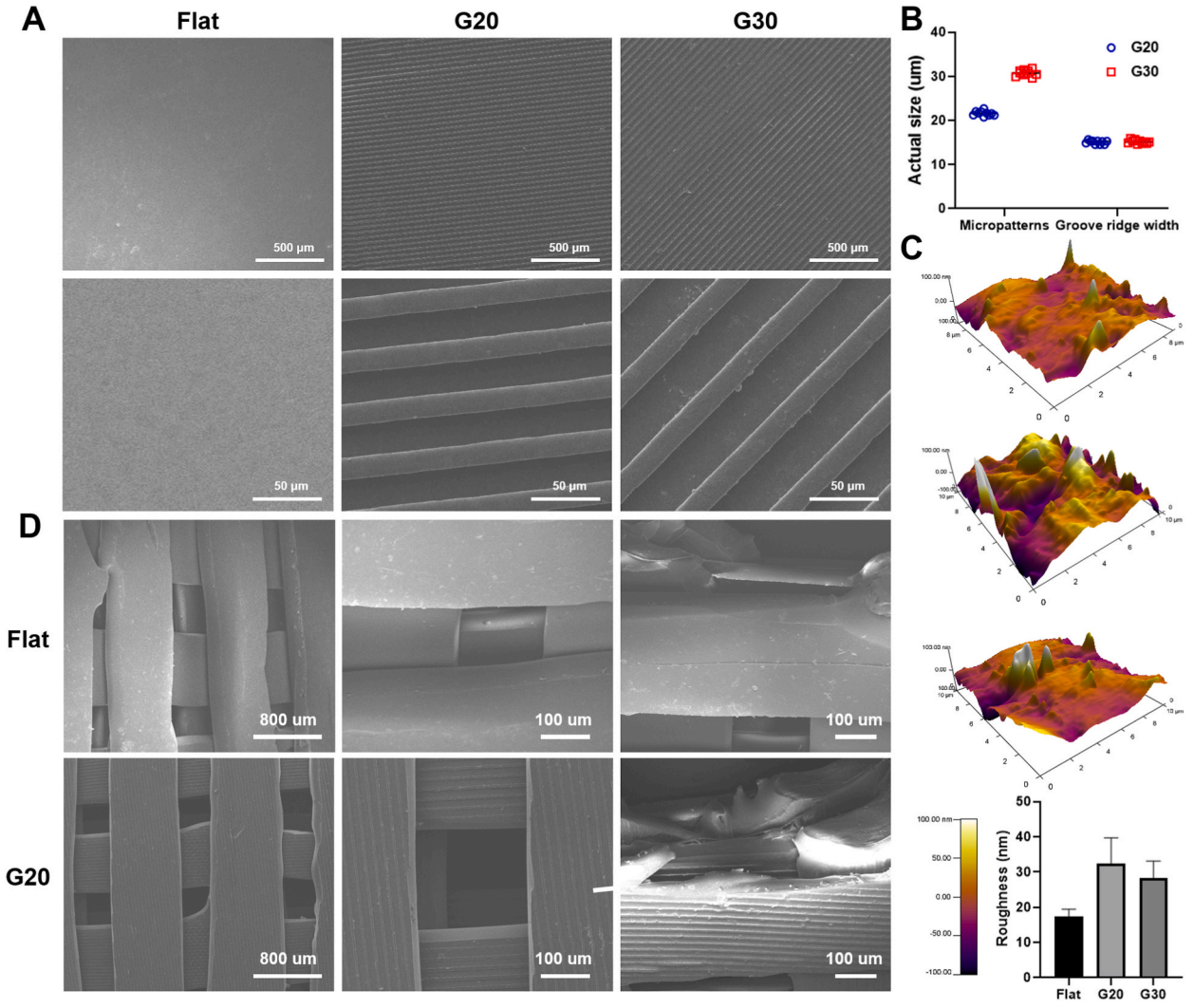

Fig. 1. Surface morphology of the materials (Falt, G20, G30). A) SEM images show the micropatterned surface structure of PCL membrane. B) Micropatterned structure dimensional quantitative analysis. C) Micropatterned surface nanomorphology and roughness analysis by AFM. D) SEM image of the topography of 3D PCL scaffolds equipped with micropatterns.

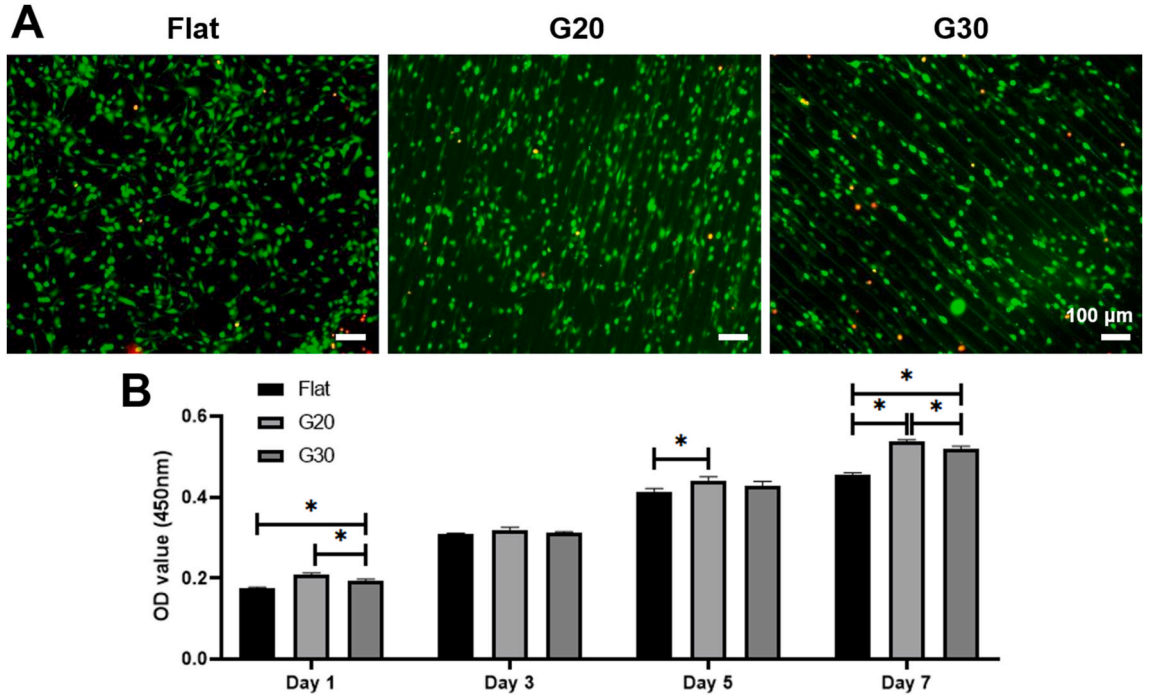

Fig. 2. Graphs of live/dead staining and proliferative activity of BMSCs in materials of Falt, G20, and G30 groups. (A) Results of live/dead staining of BMSCs co-cultured with the materials for 3 days. (B) Proliferative activity of BMSCs on the materials for 1, 3, 5, and 7 days.

the widths of the groove ridges (the plane of the grating strips) are the same. This indicates that different sizes of grating array micropatterns were successfully prepared on PCL material using the hot melt imprinting method. From Fig. 1. C, it can be seen that different sizes of grating arrays affect the surface nanomorphology of PCL materials, and it can be seen that the surface prepared micropatterns have similar morphology and roughness on the surface nano-levels of the materials with smooth surfaces, and the nanomorphology and roughness are almost the same between different micropatterns.

To further observe the surface micromorphology of the obtained scaffolds, we chose the flat group (Flat) and the grating group (G20) and used SEM to characterize the scaffolds (Fig. 1. D). The scaffolds in the Flat group had a flat and smooth surface morphology, and the same was true for the scaffolds on the lateral side of the scaffolds, with only melt-bonding occurring at the inter-layer connection of the scaffolds by hot-melting, while the scaffolds in the G20 group had a clear surface morphology on the surface and lateral side of the scaffolds. The surface and side morphology of the G20 group can be observed on the fiber surface between the layers of different stents, the grating arrays are well structured, and the surface structure of the stents will not be damaged extensively by connecting the layers of the stents by high-temperature spot hot-melting in the process of stent preparation, and the fusion bonding occurs only at the connection area. This indicates that we have successfully prepared three-dimensional scaffolds with controllable micropatterns.

In addition, we measured the porosity of the material in the G20 group to be 71.6% ± 1.3 and the shear strength to be 1.72 MPa ±0.12. Noteworthily, the porosity and the shear strength of the Flat and G30 groups are similar to those of the G20 group, and therefore the data are not shown.

3.2. Proliferation activity of BMSCs on different materials

As shown in Fig. 2. B, on day 1, the proliferative activity of BMSCs in the grating group was slightly more significant than that in the Falt group, while the OD value of the G20 group was slightly higher than that of the G30 group. There was no significant difference in the OD values of the three groups on the third day, which was consistent with the results of live-dead staining (Fig. 2. A), and the number of active cells (green fluorescence) was not significantly different among the three groups, with almost no dead cells (red fluorescence). Notably, compared to the haphazard arrangement of BMSCs in the Falt group, the proliferation of BMSCs in the grating group was distributed along the grating walk, which further suggests that materials with surface micropatterns can modulate cell growth behavior. The cell proliferation of each group increased with the increase of incubation time, and the difference of each group was consistent with that of day 5 and day 1, however, by day 7, The proliferation of BMSCs was significantly accelerated in the G20 group compared with the G30 group, while the grating group was significantly higher than the Falt group.

3.3. Possessing grating array micropatterned PCL materials modulates osteogenic differentiation of BMSCs

The results of grating array micropatterning on the regulation of osteogenic differentiation-related genes (ALP, COL1, RUNX2) in BMSCs are shown in Fig. 3. A1, A2. At the early stage of osteogenic differentiation, only the expression of genes (RUNX2, COL1, and ALP) in the G20 group showed significant up-regulation compared to that in the Flat group. in the G30 group, only the ALP gene showed significant up-regulation, and the expression of COL1 and RUNX2 genes was significantly lower than that in the Falt group. On day 14, G20 was significantly higher than the remaining two groups in each gene expression. In ALP expression the Falt group was significantly up-regulated, but still slightly lower than the G30 group, while the expression of the COL1 gene was not significantly different between the two groups. The expression of RUNX2 in the G30 group was significantly up-regulated at day 14, higher than that in the Falt group. Taken together, grating micropatterns regulated the expression of osteogenesis-related genes in BMSCs significantly higher in the grating group than in the planar group, with the G20 group being the best. BMSCs were inoculated on the surface of lenticular micropatterns, and ALP quantitative analysis was performed at 7 and 14 days of osteogenesis induction (Fig. 3. B). On day 7, ALP activity was most significant in the G20 group, while there was no significant difference between the G30 group and the Falt group, and on day 14, ALP expression of each group appeared to be increased to a certain extent, with the lenticular group being significantly higher than that of the Falt group, and the expression of which showed a decreasing trend of G20>G30>Flat. Alizarin red staining was performed after 14 days of osteogenic induction, as shown in Fig. 3. C1, the amount of mineralized calcium nodules formed on the surface of grating micropatterns was significantly more than that of the Flat group, in which the G20 group formed the most calcium nodules. The results of the quantitative analysis of alizarin red (Fig. 3. C2) were consistent with the trend of ALP expression. In summary, compared with the Flat group, PCL with grating array micropatterns significantly promoted the expression of ALP. patterned PCL significantly promoted osteogenic differentiation of BMSCs.

3.4. RAW264.7 cell proliferation activity on different materials

Fig. 4. A shows the photo of live/dead cell fluorescence staining of RAW264.7 cells cultured on Falt, G20, and G30 groups on day 3. As can be seen from the figure, the cells in the micropatterned group still proliferated along the grating array, G20 had a more significant number of live cells (green fluorescence) and almost no dead cells (red fluorescence), and G30 had a non-significant difference in the proliferation of the live cells compared to the Falt group, but the number of dead cells was slightly higher. In the cell proliferation activity assay on days 1, 3, 5, and 7 (Fig. 4. B), the difference between the three groups of materials in the proliferation activity assay on the first day was not significant, and the OD value of the grating group was slightly higher than that of the Falt group on days 3 and 5, and with the increase of co-cultivation time, the OD value of each group was up-regulated, and the OD value of the grating group was more significantly up-regulated on the 7th day, and in general, the RAW264.7 cell proliferation activity of the material on the proliferative activity G20>G30>Flat.

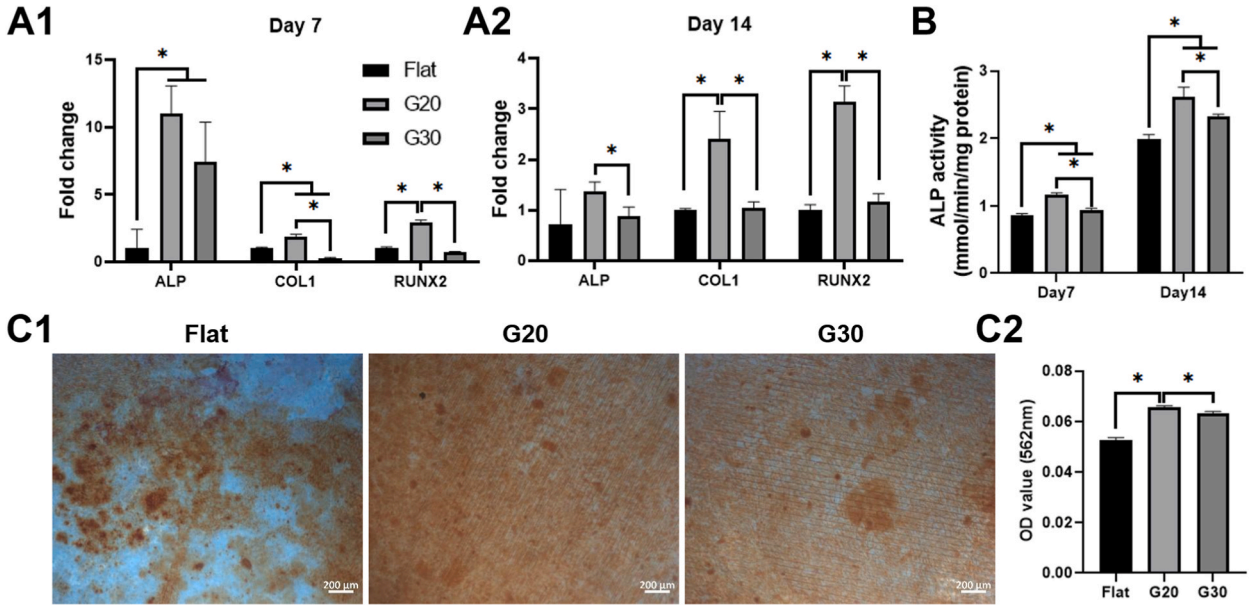

Fig. 3. Osteogenic differentiation of BMSCs on Falt, G20, and G30 materials.(A1, A2) BMSCs Expression of bone-related genes on days 7 and 14. (B) ALP quantification on days 7 and 14. (C1, C2) Calcium nodule staining and quantification on day 14.

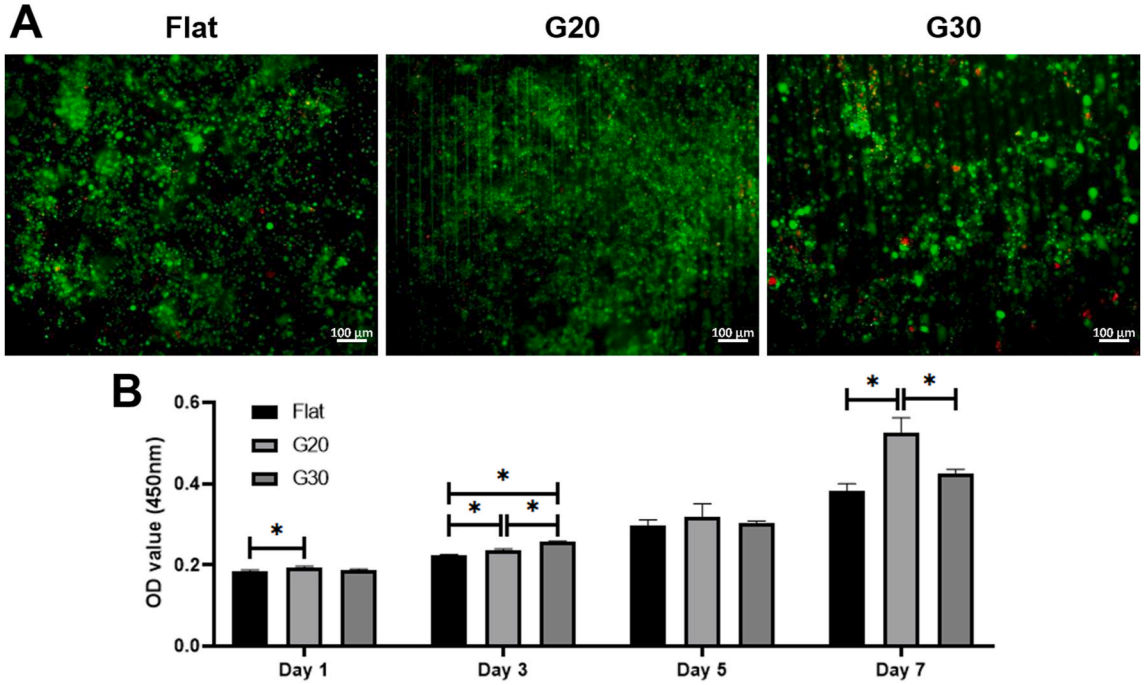

Fig. 4. Live/dead staining and proliferative activity plots of RAW264.7 cells. A) Results of live/dead staining of RAW264.7 cells co-cultured with Falt, G20, and G30 for 3 days. B) Proliferative activity of RAW264.7 cells on Falt, G20, and G30 on days 1, 3, 5, and 7.

3.5. Grating array micropatterned immunomodulation of RAW264.7 cell polarization

The regulation of M2 type marker genes IL-10, Arginase, and TGF-β1 by the grating array pattern structure in RAW264.7 cells is shown in Fig. 5. A1 and A2. There was no significant dominance of the grating group in the expression of the IL-10 gene on day 1, and G30 was slightly lower than that of Flat, On day 3, the G20 group was significantly up-regulated, which was higher than that of the Flat group, but the expression of the G30 group decreased and was significantly lower than Flat group. On day 1, the Arginase gene expression was significantly higher in the Great group than in the Falt group, and by day 3, it was significantly down-regulated in the G30 group. The expression of TGF-β1 was most significant in G20 at both time points, followed by the Flat group. In the expression of pro-inflammatory genes, the expression of TNF-α on day 1 was not different between G20 and Flat but was significantly upregulated in G30. Compared to the other two groups, iNOS and day 3 TNF-α expression G20 showed significant downregulation, while the Flat group was lower than the G30 group. This indicated that the G20 group significantly inhibited the release of pro-inflammatory factors and promoted the repair and remodeling of tissues. The percentage of macrophage M1-type marker CD11c in the grating micropatterned structures was quantified by flow cytometry (Fig. 5. C1, D1). The average macrophage M1 phenotype occupancy detected in the grating group was significantly lower than that in the Flat group, while it was significantly higher in the G30 group than in the G20 group. As shown in Fig. 5. C2, D2, in the quantification of macrophage M2 phenotype marker CD206 expression, the G20 group had a significantly higher percentage than the remaining groups, while the Flat group was higher than the G30 group. In summary, the micropatterning of the G20 group had a promoting effect on macrophage M2 polarization and its phenotypic transformation after M2 polarization, and also effectively inhibited the expression of M1-related inflammatory factors and reduced the inflammatory response of cells.

4. Discussion

PCL is easy to synthesized and surface-modified aliphatic polyester, with good biocompatibility and slow degradation characteristics, which can provide long-term support media for bone defect repair, and has been widely used in bone tissue engineering [28]. However, PCL is not biologically active, and its application as a bone repair material usually requires surface modification, composite bioceramics, or drug loading [29,30]. The micro-patterned structures have also been shown to be biologically inactive. In addition, it has been shown that micropatterned structures with sizes in the range of 20–60 μm not only support macrophage immunophenotypic modulation, but also regulate the adhesion, proliferation, and differentiation of BMSCs [24,26,31]. Based on these, we used PCL as a matrix material and modified its surface by soft lithography and 3D printing to prepare PCL membrane sheets with sizes of 21.60 ± 0.56 μm (G20), 30.76 ± 0.72 μm grating array PCL membrane sheets and 3D scaffolds with internal controllable micropatterning (Fig. 1. B). By analyzing the nanomorphology of the material surfaces, the three groups of materials had similar morphology and roughness at the nanoscale, which indicated that the variability of different micropatterned surfaces at the nanometer level was much

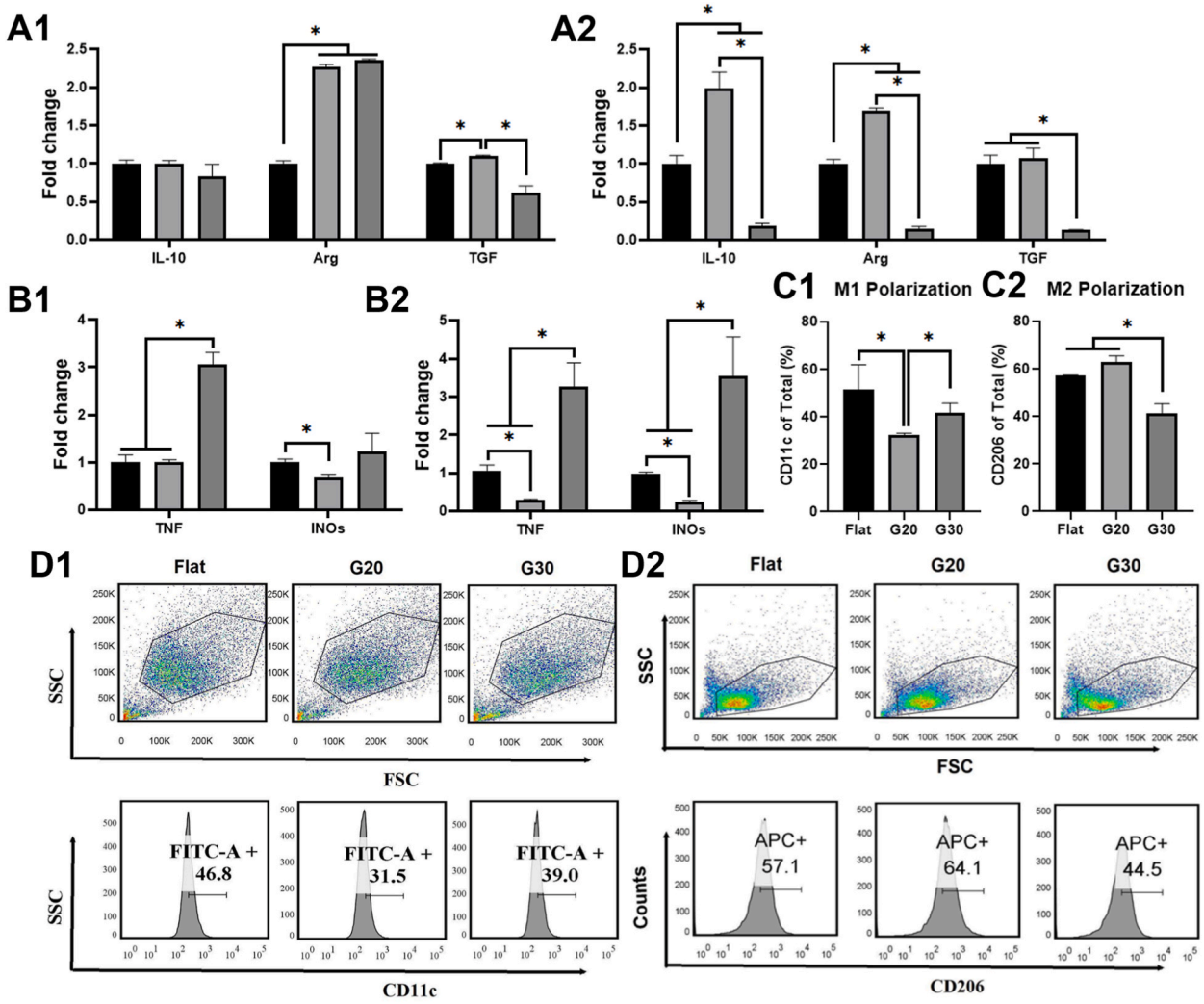

Fig. 5. Pictures of grating micropatterns regulating the polarization of RAW264.7 cells. (A1, A2) Grating micropatterns regulating the expression of genes related to the 1st and 3rd day of RAW264.7 cells polarized towards M2. B1, B2) Grating micropatterns regulating the expression of genes related to the 1st and 3rd day of RAW264.7 cells polarized towards M1. C1, C2, D1, D2) the flow cell analysis and result graphs after 1 day of incubation with the surface of Grating micropatterns. days after flow cytometric analysis and result plots.

less than that at the micrometer level (Fig. 1. C). This further highlights the stability of our process for preparing the material, in line with the design concept of micrometer-scale size differences. Notably, the perception of physical characteristics of the extracellular matrix has a profound impact on the activity and fate of adherent cells, such as BMSCs and macrophages can adjust the envelope curvature by sensing the micro- and nano-morphological changes of the external environment during the adherence to the material to cause the opening of the target ion channels or the alteration of the protein conformation and convert the mechanical signal into the conducting signal to guide the cell proliferation, migration, differentiation, and even cell death [32–34].To this end, we co-cultured three groups of materials, Flat, G20, and G30, with BMSCs and RAW264.7 cells, respectively. Their cell proliferation results similarly confirmed this conclusion and the proliferative activity of the two types of cells with grating-arrayed micropatterns was superior to that of the Flat group. The smaller-sized grating arrays (G20) having a significant proliferative effect on the cells of the larger sizes (G30), which was consistent with a previous study [35]. This may be due to the fact that the G20 group contained grating micropatterns with the smallest grating spacing and had the greatest surface roughness compared to the Flat and G30 groups, which was most favorable for cell adhesion and proliferation [36]. In the live/dead staining results on day 3 of co-culture, we found that the micropatterned material could regulate the distribution of cells along the grating shape direction(Orientation of cells on the surface of grating group material), which further demonstrated that the micro- and nanostructures of the material would affect the direction, morphology, and skeleton of cell proliferation [37].

In terms of contributing to bone differentiation properties, the grating group materials performed equally significantly, but the different sizes of grating structures had different regulatory properties on BMSCs. the G20 group up-regulated the expression of

osteogenic genes significantly, including ALP, COL1, and RUNX2, and was similarly superior to the G30 group in terms of the expression of ALP as well as calcium nodules (Fig. 3). It' s also due to the fact that the high density of raster groove ridges (the roughest surface) in the G20 group facilitates the adhesion and differentiation of BMSCs [36]. In terms of immunomodulation, the G20 group resulted in significant upregulation of macrophage M2-type genes (IL-10, Arginase, TGF-β1) and the marker CD206, while effectively suppressing the expression of M1-type genes (TNF-α, iNOS) and the marker CD11C (Fig. 5). Macrophages are the main immune effector cells in bone repair, and the main role of M1 type is to promote the early inflammatory response to trauma, which facilitates the clearance of foreign bodies or pathogens. And the predominance of M1-type macrophages after the implantation of bone filler materials can easily lead to the occurrence of immune rejection. While the main role of M2 type is to anti-inflammatory and promote tissue repair [38,39]. Macrophages are more likely to adhere to the G20-sized grating groove than to G30, and the widening of the size is not conducive for macrophages from extending into the grating strips on either side of the groove by regulating actin pseudopods [40]. Notably, the degree of macrophage stretch correlated with the expression of M2 phenotypic markers, which may account for the fact that G20 was more able to modulate macrophage M2 polarization than Flat and G30 in this study G20 is also a good choice for the regulation of M2 polarization in macrophages [41,42]. Therefore, bone repair materials with the ability to modulate macrophage M1 to M2 polarization can provide a suitable immune microenvironment for osteogenesis and accelerate the bone regeneration process.

In conclusion, the G20-sized grating array structure possesses immunomodulatory and coordinated osteogenic properties, and the integration of micropatterned structures into 3D scaffolds by combining 3D printing and soft lithography is expected to successfully reproduce scaffolds with good functionality of tissues or alternative tissue functions [43–45]. However, this study did not explore the effects of grating structures in a wider range of sizes on BMSCs and macrophages and lacked in vivo experiment. In the next step, we will further explore more size ranges of grating structures on cells as well as perform in vivo experimental validation.

5. Conclusion

In this study, the PCL surface was modified by combining soft lithography and 3D printing technology, and 3D scaffolds with internal stable and controllable structure and clear grating array structure were prepared successfully. This kind of scaffold with good cytocompatibility can not only promote the osteogenic differentiation of BMSCs but also provide a good immune environment for bone regeneration, which could reduce inflammation and accelerate the regeneration of bone tissues. It is a step forward in the exploration of bone filler materials, which can make a new contribution to the provision of high-quality materials.

Data availability statement

Sharing research data helps other researchers evaluate your findings, build on your work and to increase trust in your article. We encourage all our authors to make as much of their data publicly available as reasonably possible. Please note that your response to the following questions regarding the public data availability and the reasons for potentially not making data available will be available alongside your article upon publication.

Has data associated with your study been deposited into a publicly available repository?

Response: No.

Please select why. Please note that this statement will be available alongside your article upon publication.

Response: Data will be made available on request.

CRediT authorship contribution statement

Weihua Huang: Writing – original draft, Project administration, Methodology, Investigation. **Xiayu Cai:** Project administration, Methodology, Investigation, Data curation, Conceptualization. **Chujie Xiao:** Project administration. **Wenlu Song:** Project administration. **Huinan Yin:** Project administration. **Weikang Xu:** Writing – review & editing, Project administration, Funding acquisition, Data curation, Conceptualization.

Declaration of competing interest

The authors declare that they have no known competing financial interests or personal relationships that could have appeared to influence the work reported in this paper.

References

[1] M.S.G. Farashah, M. Javadi, A. Mohammadi, J.S. Rad, S.K. Shakouri, L. Roshangar, Bone marrow mesenchymal stem cell's exosomes as key nanoparticles in osteogenesis and bone regeneration: specific capacity based on cell type, Mol. Biol. Rep. 49 (2022) 12203–12218, https://doi.org/10.1007/s11033-022-07807-1.

[2] B. Kristjansson, S. Honsawek, Current perspectives in mesenchymal stem cell therapies for osteoarthritis, Stem Cell. Int. (2014), https://doi.org/10.1155/2014/194318, 2014.

[3] N. Yang, Y. Liu, The role of the immune microenvironment in bone regeneration, Int. J. Med. Sci. 18 (2021) 3697–3707, https://doi.org/10.7150/ijms.61080.

[4] M. Wu, H. Liu, Y. Zhu, F. Chen, Z. Chen, L. Guo, P. Wu, G. Li, C. Zhang, R. Wei, L. Cai, Mild photothermal-stimulation based on injectable and photocurable hydrogels orchestrates immunomodulation and osteogenesis for high-performance bone regeneration, Small 19 (2023), https://doi.org/10.1002/smll.202300111.

[5] R. Branemark, L. Emanuelsson, A. Palmquist, P. Thomsen, Bone response to laser-induced micro- and nano-size titanium surface features, Nanomed. Nanotechnol. Biol. Med. 7 (2011) 220–227, https://doi.org/10.1016/j.nano.2010.10.006.

[6] P. Slepicka, N.S. Kasalkova, J. Siegel, Z. Kolska, L. Bacakova, V. Svorcik, Nano-structured and functionalized surfaces for cytocompatibility improvement and bactericidal action, Biotechnol. Adv. 33 (2015) 1120–1129, https://doi.org/10.1016/j.biotechadv.2015.01.001.

[7] R. Peng, X. Yao, J. Ding, Effect of cell anisotropy on differentiation of stem cells on micropatterned surfaces through the controlled single cell adhesion, Biomaterials 32 (2011) 8048–8057, https://doi.org/10.1016/j.biomaterials.2011.07.035.

[8] H. Byun, Y.B. Lee, E.M. Kim, H. Shin, Fabrication of size-controllable human mesenchymal stromal cell spheroids from micro-scaled cell sheets, Biofabrication 11 (2019), https://doi.org/10.1088/1758-5090/ab21f6.

[9] N.R.M. Beijer, Z.M. Nauryzgaliyeva, E.M. Arteaga, L. Pieuchot, K. Anselme, J. van de Peppel, A.S. Vasilevich, N. Groen, N. Roumans, D.G.A.J. Hebels, J. de Boer, Dynamic adaptation of mesenchymal stem cell physiology upon exposure to surface micropatterns, Sci. Rep. 9 (2019), https://doi.org/10.1038/s41598-019-45284-y.

[10] A. Moreira, S. Madeira, M. Buciumeanu, J. Fialho, A. Carvalho, F. Silva, F.J. Monteiro, J. Carames, Design and surface characterization of micropatterned silica coatings for zirconia dental implants, J. Mech. Behav. Biomed. Mater. 126 (2022), https://doi.org/10.1016/j.jmbbm.2021.105060.

[11] J. Wang, Y. Su, L. Xu, D. Li, Micro-patterned surface construction on BCP ceramics and the regulation on inflammation-involved osteogenic differentiation, Mater. Sci. Eng., C 116 (2020), https://doi.org/10.1016/j.msec.2020.111220.

[12] B. Tüzün-Antepli, Ş. Şeker, A. Elçin, G. Khang, Y.J.M. Elçin, Evaluation of human osteoblasts on NIPS micro-patterned PCL carriers containing nanohydroxyapatite and reduced graphene Oxide using PSμM, Molecules 27 (2022), https://doi.org/10.3390/molecules27207091.

[13] H. Otsuka, Nanofabrication technologies to control cell and tissue function in three-dimension, Gels 9 (2023), https://doi.org/10.3390/gels9030203.

[14] C. Zhang, Z. Zhou, N. Liu, J. Chen, J. Wu, Y. Zhang, K. Lin, S. Zhang, Osteogenic differentiation of 3D-printed porous tantalum with nano-topographic modification for repairing craniofacial bone defects, Front. Bioeng. Biotechnol. 11 (2023), https://doi.org/10.3389/fbioe.2023.1258030.

[15] A. Prasopthum, K.M. Shakesheff, J. Yang, Direct three-dimensional printing of polymeric scaffolds with nanofibrous topography, Biofabrication 10 (2018), https://doi.org/10.1088/1758-5090/aaa15b.

[16] A. Mata, E.J. Kim, C.A. Boehm, A.J. Fleischman, G.F. Muschler, S. Roy, A three-dimensional scaffold with precise micro-architecture and surface micro-textures, Biomaterials 30 (2009) 4610–4617, https://doi.org/10.1016/j.biomaterials.2009.05.023.

[17] G. Hochleitner, T. Juengst, T.D. Brown, K. Hahn, C. Moseke, F. Jakob, P.D. Dalton, J. Groll, Additive manufacturing of scaffolds with sub-micron filaments via melt electrospinning writing, Biofabrication 7 (2015), https://doi.org/10.1088/1758-5090/7/3/035002.

[18] J.Z. Yu, E. Korkmaz, M.I. Berg, P.R. LeDuc, O.B. Ozdoganlar, Biomimetic scaffolds with three-dimensional undulated microtopographies, Biomaterials 128 (2017) 109–120, https://doi.org/10.1016/j.biomaterials.2017.02.014.

[19] Y.-M. Kook, Y. Jeong, K. Lee, W.-G. Koh, Design of biomimetic cellular scaffolds for co-culture system and their application, J. Tissue Eng. 8 (2017), https://doi.org/10.1177/2041731417724640.

[20] C. Mas-Moruno, B. Su, M.J.A.h.m. Dalby, Multifunctional coatings and nanotopographies: toward cell instructive and antibacterial implants, Adv. Healthcare Mater. 8 (2019) e1801103, https://doi.org/10.1002/adhm.201801103.

[21] A. Kosik-Koziol, E. Graham, J. Jaroszewicz, A. Chlanda, P.T.S. Kumar, S. Ivanovski, W. Swieszkowski, C. Vaquette, Surface modification of 3D printed polycaprolactone constructs via a solvent treatment: impact on physical and osteogenic properties, ACS Biomater. Sci. Eng. 5 (2019) 318, https://doi.org/10.1021/acsbiomaterials.8b01018. -+.

[22] M. Gharibshahian, M. Salehi, N. Beheshtizadeh, M. Kamalabadi-Farahani, A. Atashi, M.-S. Nourbakhsh, M. Alizadeh, Recent advances on 3D-printed PCL-based composite scaffolds for bone tissue engineering, Front. Bioeng. Biotechnol. 11 (2023), https://doi.org/10.3389/fbioe.2023.1168504.

[23] M.S. Laranjeira, A. Carvalho, A. Pelaez-Vargas, D. Hansford, M.P. Ferraz, S. Coimbra, E. Costa, A. Santos-Silva, M.H. Fernandes, F.J. Monteiro, Modulation of human dermal microvascular endothelial cell and human gingival fibroblast behavior by micropatterned silica coating surfaces for zirconia dental implant applications, Sci. Technol. Adv. Mater. 15 (2014), https://doi.org/10.1088/1468-6996/15/2/025001.

[24] J.D. Bryers, C.M. Giachelli, B.D. Ratner, Engineering biomaterials to integrate and heal: the biocompatibility paradigm shifts, Biotechnol. Bioeng. 109 (2012) 1898–1911, https://doi.org/10.1002/bit.24559.

[25] A. Wilkinson, R.N. Hewitt, L.E. McNamara, D. McCloy, R.M.D. Meek, M.J. Dalby, Biomimetic microtopography to enhance osteogenesis in vitro, Acta Biomater. 7 (2011) 2919–2925, https://doi.org/10.1016/j.actbio.2011.03.026.

[26] X. Wang, T. Nakamoto, I. Dulinska-Molak, N. Kawazoe, G. Chen, Regulating the stemness of mesenchymal stem cells by tuning micropattern features, J. Mater. Chem. B 4 (2016) 37–45, https://doi.org/10.1039/c5tb02215k.

[27] T. Tylek, C. Blum, A. Hrynevich, K. Schlegelmilch, T. Schilling, P.D. Dalton, J. Groll, Precisely defined fiber scaffolds with 40 μm porosity induce elongation driven M2-like polarization of human macrophages, Biofabrication 12 (2020) 025007, https://doi.org/10.1088/1758-5090/ab5f4e.

[28] N. Siddiqui, S. Asawa, B. Birru, R. Baadhe, S. Rao, PCL-based composite scaffold matrices for tissue engineering applications, Mol. Biotechnol. 60 (2018) 506–532, https://doi.org/10.1007/s12033-018-0084-5.

[29] H. Hosseinkazemi, E. Biazar, S. Bonakdar, M.-T. Ebadi, M.-A. Shokrgozar, M. Rabiee, Modification of PCL electrospun nanofibrous mat with Calendula officinalis extract for improved interaction with cells, International Journal of Polymeric Materials and Polymeric Biomaterials 64 (2015) 459–464, https://doi.org/10.1080/00914037.2014.958835.

[30] C. Cao, P. Huang, A. Prasopthum, A.J. Parsons, F. Ai, J. Yang, Characterisation of bone regeneration in 3D printed ductile PCL/PEG/hydroxyapatite scaffolds with high ceramic microparticle concentrations, Biomater. Sci. 10 (2021) 138–152, https://doi.org/10.1039/d1bm01645h.

[31] A. Wilkinson, R.N. Hewitt, L.E. McNamara, D. McCloy, R.M.D. Meek, M.J. Dalby, Biomimetic microtopography to enhance osteogenesis in vitro, Acta Biomater. 7 (2011) 2919–2925, https://doi.org/10.1016/j.actbio.2011.03.026.

[32] V. Vogel, M. Sheetz, Local force and geometry sensing regulate cell functions, Nat. Rev. Mol. Cell Biol. 7 (2006) 265–275, https://doi.org/10.1038/nrm1890.

[33] N.S. Gov, A. Gopinathan, Dynamics of membranes driven by actin polymerization, Biophys. J. 90 (2006) 454–469, https://doi.org/10.1091/mbc.E16-04-0253.

[34] D. Geblinger, L. Addadi, B. Geiger, Nano-topography sensing by osteoclasts (vol 123, pg 1503, 2010), J. Cell Sci. 123 (2010), https://doi.org/10.1242/jcs.073411, 1814-1814.

[35] T. Marques-Almeida, V.F. Cardoso, M. Gama, S. Lanceros-Mendez, C. Ribeiro, Patterned piezoelectric scaffolds for osteogenic differentiation, Int. J. Mol. Sci. 21 (2020), https://doi.org/10.3390/ijms21218352.

[36] Y. Hou, L. Yu, W. Xie, L.C. Camacho, M. Zhang, Z. Chu, Q. Wei, R. Haag, Surface roughness and substrate stiffness synergize to drive cellular mechanoresponse (vol 20, pg 748, 2020), Nano Lett. 20 (2020), https://doi.org/10.1021/acs.nanolett.0c01294, 4059-4059.

[37] E. Martinez, E. Engel, J.A. Planell, J. Samitier, Effects of artificial micro- and nano-structured surfaces on cell behaviour, Annals of Anatomy-Anatomischer Anzeiger 191 (2009) 126–135, https://doi.org/10.1109/ICAET.2014.7105301.

[38] T. Roszer, Understanding the Mysterious M2 Macrophage through Activation Markers and Effector Mechanisms, Mediators of Inflammation, 2015, p. 2015, https://doi.org/10.1155/2015/816460.

[39] F.O. Martinez, S. Gordon, The M1 and M2 paradigm of macrophage activation: time for reassessment, F1000prime reports 6 (2014), https://doi.org/10.12703/P6-13, 13-13.

[40] Q. Gao, C. Xie, P. Wang, M. Xie, H. Li, A. Sun, J. Fu, Y. He, 3D printed multi-scale scaffolds with ultrafine fibers for providing excellent biocompatibility, Mater. Sci. Eng., C 107 (2020), https://doi.org/10.1016/j.msec.2019.110269.

[41] T.U. Luu, Shannon C. Gott, Bryan W.K. Woo, Masaru P. Rao, Wendy F. Liu, Micro and nano-patterned topographical cues for regulating macrophage cell shape and phenotype, ACS Appl. Mater. Interfaces 51 (2015) 28665–28672, https://doi.org/10.1021/acsami.5b10589.

[42] F.Y. McWhorter, T. Wang, N. Phoebe, C. Thanh, W.F. Liu, Modulation of macrophage phenotype by cell shape, Proc. Natl. Acad. Sci. U.S.A. 110 (2013) 17253–17258, https://doi.org/10.1073/pnas.1308887110.

[43] T. Wu, S. Yu, D. Chen, Y. Wang, Bionic design, materials and performance of bone tissue scaffolds, Materials 10 (2017), https://doi.org/10.3390/ma10101187.
[44] K. Wang, X. Wang, C. Han, W. Hou, J. Wang, L. Chen, Y. Luo, From micro to macro: the hierarchical design in a micropatterned scaffold for cell assembling and transplantation, Adv. Mater. 29 (2017) 1604600–1604601, https://doi.org/10.1002/adma.201604600, 1604600.7.
[45] J. Shi, L. Zhu, L. Li, Z. Li, J. Yang, X. Wang, A TPMS-based method for modeling porous scaffolds for bionic bone tissue engineering, Sci. Rep. 8 (2018) 7395, https://doi.org/10.1038/s41598-018-25750-9.